Wang *et al. Biochar* (2026) 8:97
https://doi.org/10.1007/s42773-026-00604-0

Biochar

ORIGINAL RESEARCH Open Access

Heat loss and water transport capacity regulation in hybrid evaporators

Sihui Wang[1], Jiaqi Yang[1], Aijie Wang[1] and Wenzong Liu[1*]

Abstract

Solar interface evaporation technology, as a green and low-carbon water treatment solution, faces the core challenge of how to co-optimize photothermal conversion, water transport, and energy management through material design. Hydrogels have attracted significant attention for their hydrophilic networks and unique water molecular states in the field of solar interface evaporation. However, the mechanisms behind their improvement and efficiency enhancement remain unclear. We demonstrated that biochar doping improves the photothermal performance of hydrogels, regulates water absorption and transport, and reduces evaporation enthalpy. The dual photothermal and non-photothermal pathway enhancement mechanisms of functional groups are revealed. It is illustrated that the interaction between biochar and polymer chains changes the pore structure of hybrid hydrogels, promoting light absorption and water transport. Furthermore, the surface functional groups of biochar interact with hydrogen bond networks, increasing IW/FW and effectively enhancing water evaporation capacity. By combining enhanced photothermal performance, hydrophilicity, water transport capabilities, and lowered evaporation enthalpy, the incorporation of biochar comprehensively boosts the evaporation rate of hybrid hydrogels.

Highlights

- Photothermal and non-photothermal mechanisms were revealed in biochar-doped hybrid hydrogels.
- An impressive evaporation rate of 3.57 kg m^{-2} h^{-1} was achieved under one sun with an improved water transport capacity and light absorption.
- Interfacial water content increase reduced the evaporation enthalpy to a very low level.

Keywords Hybrid hydrogel, Biochar, Solar evaporation, Synergistic mechanism, Evaporation enthalpy

*Correspondence:
Wenzong Liu
Liuwenzong@hit.edu.cn
[1]Shenzhen Key Laboratory of Organic Pollution Prevention and Control, State Key Laboratory of Urban-Rural Water Resource and Environment, School of Eco-Environment, Harbin Institute of Technology (Shenzhen), Shenzhen 518055, China.

Springer

Graphical Abstract

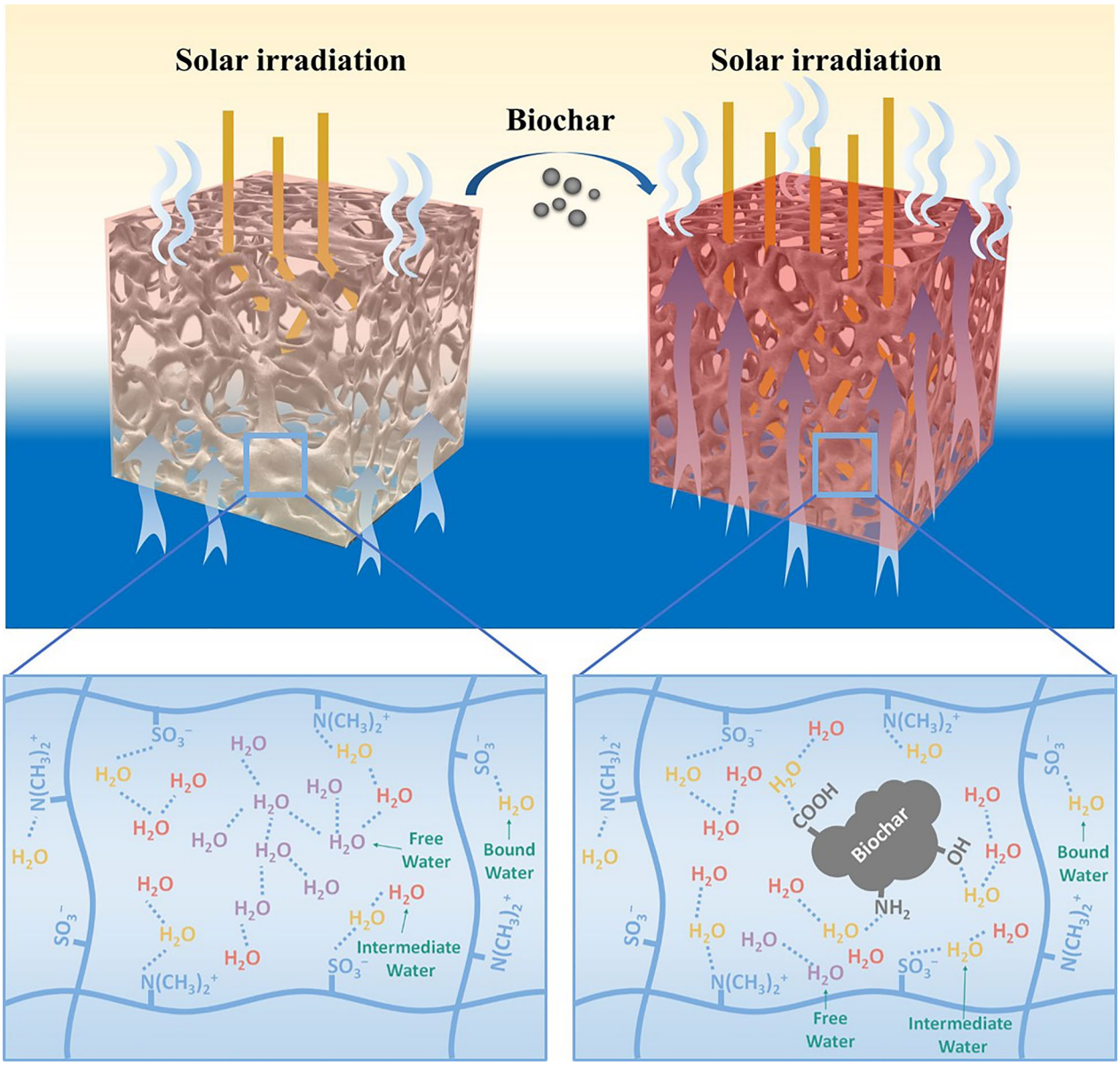

1 Introduction

Regional lack and imbalance of freshwater resources have become one of the core challenges to global sustainable development (Wang et al. 2022; Aleid et al. 2022). The majority of water on Earth is brine, including seawater and saline wastewater. Existing conventional water treatment and resource recovery technologies, such as reverse osmosis and multi-stage flash distillation, all face issues of excessive energy consumption and cost (ebrahimi et al. 2022). Interfacial evaporation using solar energy to desalinate salt water has become a proven and effective alternative solution (Alex et al. 2019; Fan et al. 2024). Using green, clean solar energy for interface evaporation of saline water has become a proven alternative solution. It combines the areas for heating and evaporation, which helps to reduce the transmission of heat to the bulk of water and improve energy efficiency and solar evaporation performance (Zhang et al. 2021). The conditions that a stable and efficient solar interface evaporator must fulfill are as follows: (1) high photothermal conversion

ability; (2) low thermal conductivity to reduce heat loss; (3) good water transport capacity; (4) resistance to salt crystallization when evaporating saline water (Liu et al. 2022; Guo et al. 2022; Lei et al. 2023).

Hydrogels, owing to the three-dimensional hydrophilic network structure, highly tunable physicochemical properties, and low evaporation enthalpy advantages, have emerged as a promising substrate for solar interface evaporation systems (Zhang and Khademhosseini 2017; Guo and Yu 2021; Guo et al. 2021). The excellent water transport capability ensures a continuous supply of sufficient water to the interface during evaporation, while the abundant porous network reduces heat convection losses (Bian et al. 2019; Wan et al. 2025). In particular, polyzwitterionic hydrogel can effectively adapt to high-salt environments thanks to the unique anti-polyelectrolyte effect, reducing the possibility of salt crystallization during evaporation, and forming more interfacial water (IW) and reducing the evaporation enthalpy, thereby enhancing the evaporation performance (Wang et al. 2025). However, their photothermal conversion capability is weak. Incorporating cost-effective photothermal materials into hydrogels with a regulated three-dimensional network structure is an efficient approach to fabricating evaporators with strong and stable light absorption performance (Liu et al. 2025). Yu et al. embedded carbon nanotubes in the hydrophilic polymer sodium alginate to prepare highly water-absorbing aerogel, achieving high light absorption rates (over 96%) with an evaporation performance of 2.25 kg m^{-2} h^{-1} (Yu et al. 2025). It indicates that higher surface temperature and evaporation efficiency can be further done when heat energy loss in the aerogel is considered and regulated.

In recent years, biochar with a wide range of sources has good porous structure, broad-spectrum absorptive properties, and chemical stability, providing notable advantages, particularly in terms of photothermal conversion efficiency and low cost, compared to semiconductors, metals, organic polymers, and other carbon-based materials (Zhang et al. 2022a, b). Biomass materials such as loofah, carrot, sugarcane, and mushroom, treated through carbonization, can achieve acceptable solar evaporation effects (Xu et al. 2017; Long et al. 2019; Zhang et al. 2022a, b). However, biochar has limited capillary water transport capacity and suffers from interfacial heat loss when used independently, making it difficult for evaporation rates to increase sustainably (Li et al. 2021a). It is for this reason that researchers have explored composite strategies combining biochar with hydrogels. For example, Rania et al. used wood chip-derived biochar to absorb and convert solar energy, combined with hydrogels to activate water, achieving an evaporation rate of 2.71 kg m^{-2} h^{-1} with the biochar-based polyacrylamide hydrogel evaporator (Tarek et al. 2023). Additionally, biochar-based hydrogels such as porous polyvinyl alcohol/biochar hydrogel and copper-carbon hydrogel have been prepared for interfacial evaporation (Li et al. 2022; Yang et al. 2023). But till now, reported studies have primarily focused on the photothermal enhancement of hydrogels by biochar, and there remains a lack of systematic understanding of mechanisms such as chemical-structural synergistic regulation of hydrogel water transport and hydrogen bond network restructuring.

By investigating changes in the state of water molecules, photothermal performance, and water transport capacity of hydrogels with and without biochar incorporation, we reveal the synergistic mechanism of both photothermal and non-photothermal pathways in the solar-driven interfacial evaporation process of hybrid hydrogels. It is demonstrated that sorghum straw biochar optimizes the pore structure of hybrid hydrogels and activates water molecules through interactions between surface functional groups and hydrogel polymer chains and hydrogen bond networks, meanwhile enhancing water transport performance and reducing equivalent evaporation enthalpy. This provides theoretical guidance and practical implications for the design and optimization of evaporators in saline environments.

2 Materials and methods

2.1 Preparation of biochar for hydrogel fabrication

In this study, sorghum straw biochar was prepared for use in hybrid hydrogel. The sorghum straw was pyrolyzed in a tube furnace (OTF-1200X-S, Kejing, China) at 600 °C for 1 h under argon atmosphere. The heating rate was 5 °C min^{-1}. After cooling to room temperature, the samples were acid washed with nitric acid, followed by DI water to neutral pH. The samples were dried and ball-milled for 24 h (High Energy Planetary Ball Mill, DECO-PBM-H-0.4 L). Then, they were sieved through a 100-mesh sieve to obtain the biochar particles.

2.2 Fabrication of hybrid hydrogel

The hydrogel used in this experiment was polyzwitterionic hydrogel, and the gel agent used was a DMAPS system. 3 g of DMAPS was dissolved in 7 g of DI water and stirred until clear. 0.048 g of APS as an initiator and 60 μL of PEGDA as a crosslinker were added to it and sonicated for 15 min. 0.1 g of biochar particles were then dispersed in 1 mL of DI water, mixed well and added to the precursor solution. Then, after adding 3 μL of TMEDA as a catalyst and aerating with nitrogen for 15 min, the gelation reaction was carried out at 90 °C for 4 h. Finally, the hybrid hydrogel was washed with DI water to remove unreacted material. The hydrogel used as a control skipped the step of adding biochar particles.

2.3 Experiments of solar evaporation

The solar interfacial evaporation experiments were conducted at 25°C and 30% humidity. A xenon sunlight simulator with a filter (AM1.5G) (PLS-SXE300+, Pofelet, China) was used as the light source, and a hand-held spectral illuminometer (HP350C, Hangzhou LCE intelligent Detection Instrument Co., Ltd., China) was used to ensure that the light intensity on the surface of the evaporator was 1000 W m^{-2}. The weight of the device during the evaporation experiment was measured in real time using an electronic balance (ME204, Mettler Toledo, USA) and recorded every 10 min, while the temperature change of the device during evaporation was monitored with the help of an infrared thermographic camera. The simulated saline water used in this experiment was a 10 wt% NaCl solution. The dark experiment was conducted by placing the devices in a dark environment with no light source for the evaporation experiment.

2.4 Characterizations

UV–Vis-NIR absorption spectra were collected using a spectrometer (Lambda 1050+, PerkinElmer, USA). The morphology of the samples was observed using a scanning electron microscope (SEM, MDTC-EQ-M57-01, Thermo Fisher Scientific, USA). The surface wettability was tested using contact angle measurements (KRUSS DSA30). Surface elements of hydrogel and biochar samples were analyzed by X-ray photoelectron spectroscopy (PHI5000VersaProbeII, ULVAC-PHI, China). Raman spectra were obtained using a laser Raman spectrometer (Invia, Renishaw, UK) excited by a 532 nm laser. Differential scanning calorimetry (DSC) measurements were obtained using a Discovery DSC instrument (DSC3, Mettler Toledo, USA).

3 Results and discussion

3.1 Enhancement of photothermal properties

As shown in Fig. 1A, the incorporation of biochar caused the hydrogel to change from transparent to black, demonstrating that the biochar was uniformly dispersed in the hydrogel matrix (Zheng et al. 2023). In addition, the UV–Vis-NIR absorption spectrum (Fig. 1B) showed that the biochar addition significantly enhanced the absorption capacity of the hydrogel over the entire wavelength range (200–2500 nm), particularly in the 380–1500 nm wavelength band. It is worth noting that SoBC-600 °C exhibited a light absorption rate exceeding 98% in the visible light range of 430–700 nm, which is of significant importance for solar evaporation. The light absorption rate of the hybrid hydrogel maintained a stable value of over 95% across the broad spectrum, and even exceeded that of biochar in the near-infrared region beyond 1000 nm. Therefore, the improvement in the hybrid hydrogel's light absorption was not only due to the photothermal properties of biochar itself, but also the result of changes in the pore structure of the hybrid hydrogel (Ghaffar et al. 2024). Figure 1C and D show the SEM images and pore size distribution of the hydrogel

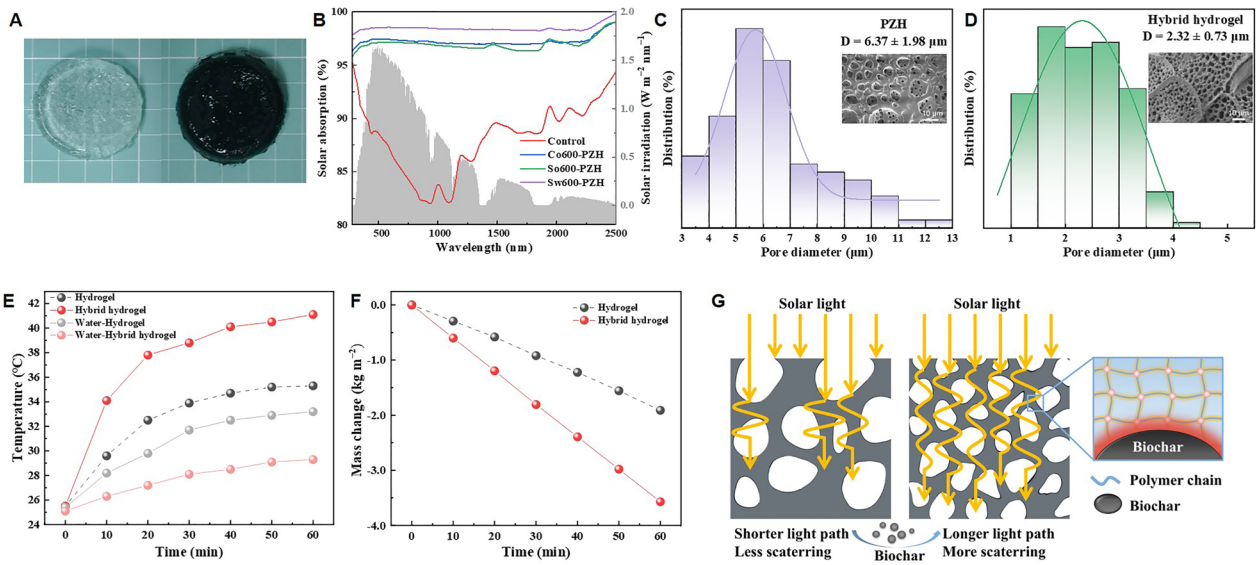

Fig. 1 Photothermal performance enhancement of hybrid hydrogel. **A** Image of hydrogel and hybrid hydrogel. **B** The optical absorption spectrum of the hydrogels and the spectrum of solar irradiation. **C** Pore size distribution and SEM images of hydrogel. **D** Pore size distribution of hybrid hydrogel. **E** The temperature changes of both the evaporation surface and bulk water under one sun irradiation. **F** The mass change of water under one sun irradiation. **G** Schematic mechanism of the effect of biochar on the photothermal properties of hybrid hydrogel

and the hybrid hydrogel, respectively. The SEM images revealed that the hybrid hydrogel possesses a denser and rougher three-dimensional network structure. The abundant microporous structure facilitates water transport and light refraction, and the biochar is completely locked and fixed within the hydrogel network structure by DMAPS, enhancing the material's mechanical stability (He et al. 2019; Li et al. 2025). The hybrid hydrogel exhibited smaller water transport pores with the connection of functional groups of biochar and hydrogel polymer chains as well as hydrogen bonds. Smaller pore sizes enable the hydrogel to have a higher light absorption rate (Fig. S2), while further increasing the surface temperature of the evaporator and accelerating the evaporation rate (Figs. S3 and S4). It is shown that smaller water transport pores also increase the internal surface area of the hydrogel, thereby increasing the probability of incident light being absorbed, while also enhancing multiple reflections and scattering of light, increasing the optical path length, and thus improving light absorption efficiency (Fan et al. 2020; Gu et al. 2024). However, excessively small pore sizes can cause pore structure collapse, thereby hindering water transport and negatively impacting evaporation rates.

By recording the heat loss of the device during evaporation and the temperature changes on the evaporator surface and water body, the effect of biochar on improving the solar evaporation performance was evaluated (Fig. 1E and F). Compared to the temperature of bulk water and the evaporator surface under irradiation, we observed an obvious enhancement on the top surface. Within one hour of light irradiation, the temperature at the control hydrogel interface gradually increased from 25.5 °C to 35.3 °C, while the water temperature also increased from 25.4 °C to 33.2 °C. Noticeably, the hybrid hydrogel interface temperature gradually increased from 25.5 °C to 41.1 °C, while the water temperature only increased from 25.1 °C to 29.3 °C, with a reduced heat dispersion around 4 °C. Furthermore, the hybrid hydrogel exhibited faster temperature rise, higher interface temperature, and almost no obvious change in the bottom water temperature (Fig. S5). This indicated that biochar hybrid enhanced the localization of photothermal conversion in the hydrogel, enabling it to rapidly convert absorbed light energy into thermal energy and confine it within the evaporator. In addition to the inherently low thermal conductivity of the hydrogel, biochar doping effectively suppressed heat conduction to the bulk water and mitigated natural convection near the evaporation interface. This was attributed to the ability of biochar to absorb sunlight and efficiently convert light energy into localized thermal energy, which promoted the evaporation of water molecules within the hydrogel rather than facilitating downward heat transfer. Furthermore, the highly porous structure of biochar significantly restricted the macroscopic movement of heated water, thereby preventing the development of large-scale thermal convection. The heat was more efficiently used to evaporate water molecules within the evaporator rather than in the bulk water, greatly reducing heat loss and improving the evaporator's photothermal and water-to-vapour conversion ability (Lei et al. 2021; Zheng et al. 2023). Higher evaporator interface temperatures and fewer heat losses result in faster evaporation rates. The evaporation rate of the hybrid hydrogel under sunlight was 3.57 kg m^{-2} h^{-1}, which was 1.87 times that of the hydrogel. This was the most direct evidence of biochar's enhancement of the evaporation efficiency of the hybrid hydrogel.

The mechanism is proposed based on the above findings (Fig. 1G). The carbon skeleton of biochar enhances the absorption of ultraviolet-visible light by hydrogels through π–π* electron transitions, thereby improving the light absorption performance of hydrogels. It also concentrates heat within the hydrogel, reducing heat loss to the bulk water. Moreover, the surface functional groups of biochar interact with the groups on the polymer chains of the hydrogel (Tarek et al. 2023). This hints that a more uniform distribution of pores and smaller pore size are supposed to be designed for light absorption regulation and heat control. Multiple reflections and the optical path length of incident light within the gel can be well extended, thereby also improving water molecule transport efficiency.

3.2 Improvement of hydrophilic and water transport properties

Hydrophilicity and water transport ability are both the critical factors for achieving efficient water evaporation and resistance to salt crystallization in solar interface evaporators. Figure 2A shows that the contact angle of the hydrogel is 64.5°, while the contact angle of the hybrid hydrogel is 17.9°, indicating that the biochar plays a significant role in improving the hydrophilicity of the hybrid hydrogel. The abundant oxygen-containing functional groups in biochar can effectively improve the hydrophilicity of hydrogel materials (Tarek et al. 2023). As shown in the XPS total spectra (Fig. 2B and C), the hydrogels were primarily composed of four elements: C, O, S, and N. With biochar addition, the C content of the hydrogel increased from 65.4% to 72.2%, verifying the successful loading of hydrophilic biochar (Ge et al. 2024). Analysis of the N1s spectrum revealed that the addition of biochar increased the diversity of nitrogen-containing organic functional groups in the hydrogel (Fig. S6). Figure 2D–F show the XPS spectra of biochar, which proved that the biochar contains hydrophilic groups, such as hydroxyl

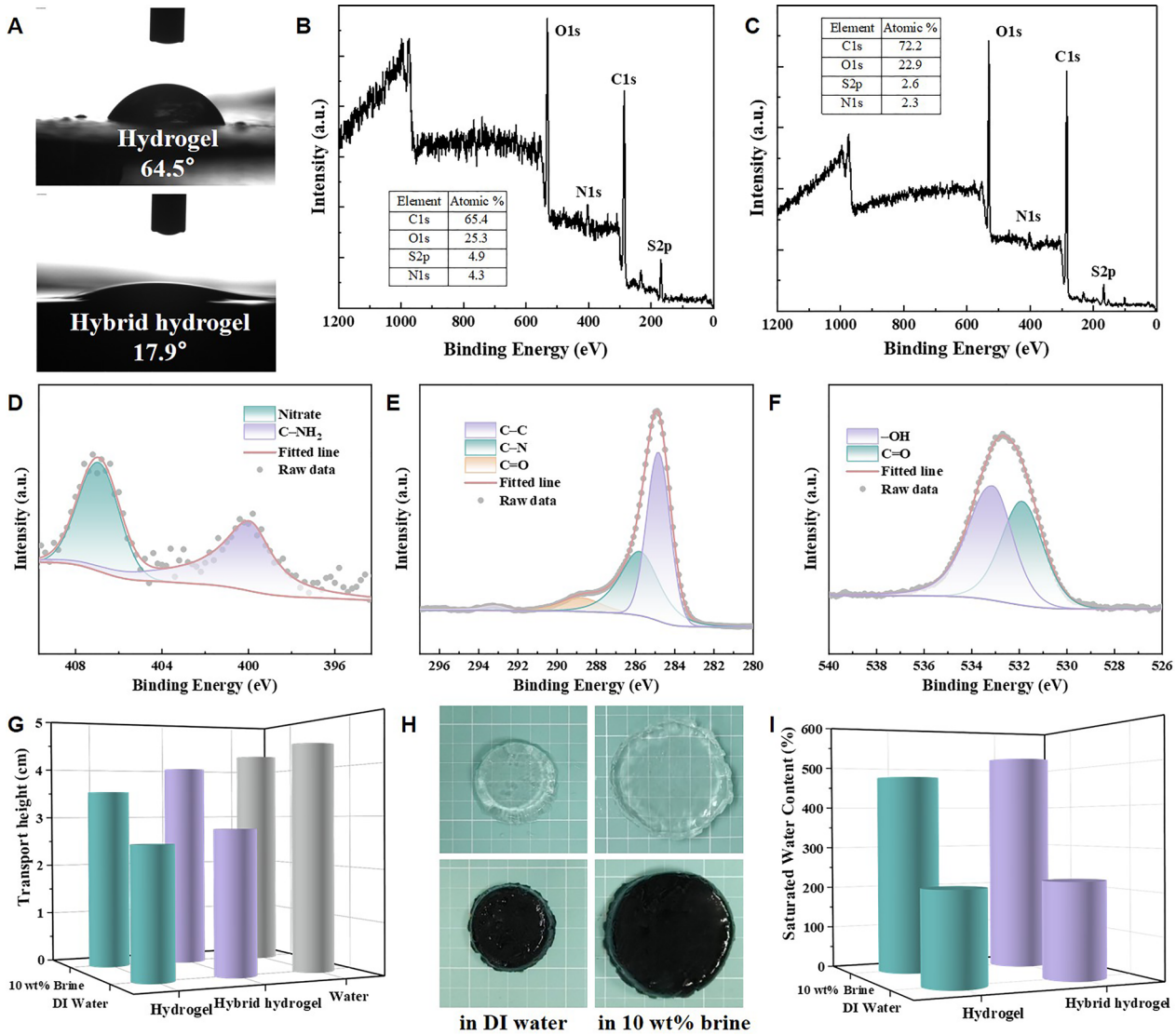

Fig. 2 Improvement of hydrophilic and water transport properties of hybrid hydrogel. **A** Contact angles of hydrogel and hybrid hydrogel. **B**, **C** The total survey XPS spectrum of hydrogel/hybrid hydrogel. **D**–**F** High-resolution XPS spectrum of C1s, O1s, and N1s of biochar. **G** Water transport height tested in pure water and 10 wt% NaCl solution of hydrogel and hybrid hydrogel. **H** Photographs of hydrogel and hybrid hydrogel after swelling in pure water and 10 wt% NaCl solution. **I** The saturated water content of hydrogel and hybrid hydrogel in pure water and 10 wt% NaCl solution

groups, amino groups, and carbonyl groups. These groups could promote the formation of hydrogen bonds between water molecules in the hydrogel as the biochar was added to the hydrogel. The total spectrum indicated that the O/C ratio of straw charcoal obtained at 600 °C reached 0.3 (Fig. S7). The high-resolution C1s spectrum of biochar exhibited three peaks at 284.8 eV, 285.8 eV, and 288.7 eV, corresponding to C–C bonds, C–N bonds, and C=O bonds, respectively. Additionally, biochar also contained hydrophilic groups such as $–NH_2$ and –OH. These groups can promote the formation of hydrogen bonds between water molecules in the hydrogel, thereby reducing the contact angle. Based on the FTIR spectrum (Fig. S8), the characteristic peaks of the hydrogel are at 1040 cm^{-1}, 1180 cm^{-1}, and 1720 cm^{-1}, corresponding to the symmetric and asymmetric stretching vibrations of S=O and the stretching vibration of C=O, respectively, confirming the formation of the hydrogel based on DMAPS (Lei et al. 2022). There were no new absorption peaks observed in the hybrid hydrogel, indicating that the interaction between biochar and DMAPS during gelation is physical in nature. Additionally, the intensity of the

hydroxyl characteristic peak at approximately 3460 cm^{-1} in the hybrid hydrogel was enhanced compared to the hydrogel, which was consistent with the enhancement of hydrogel hydrophilicity due to biochar incorporation.

The key to achieving efficient and stable operation of a solar interface evaporator depends on whether it can continuously supply sufficient amounts of water to the interface during the evaporation process. To systematically investigate the water transport performance of hydrogels, rice paper tapes were utilized as water absorbents, and the transport performance was reflected by the water transport height of the rice paper (Feng et al. 2020). The testing device is shown in Fig. S9. The hydrogel was placed in a petri dish filled with water, and the experiment began when the hydrogel's surface became wet, i.e., when the rice paper in contact with the top of the hydrogel became wetted. The water diffusion height of the rice paper was recorded over 60 min. As shown in Fig. 2G, after one hour, the hydrogel and hybrid hydrogel could transport deionized water to heights of 2.51 cm and 2.77 cm, respectively. In 10 wt% saline solution, both hydrogels exhibited improved water transport height, especially the hybrid hydrogel, achieving a transport height of 3.99 cm, which was close to the transport height (4.27 cm) when the rice paper directly contacted the saline solution. This indicates that biochar incorporation enhances the water transport performance of the hydrogel.

The swelling capacity of hydrogels is another important factor to estimate water transport capability. Figure 2H shows the morphological changes of the hydrogel without biochar and the hybrid hydrogel before and after swelling in deionized water and 10 wt% saline solution. It was observed that the hydrogel swelled more fully in the saline solution, with the diameter increasing from 4.3 cm to 6.1 cm, resulting in a larger volume. With biochar addition, the swelling volume of the hybrid hydrogel was slightly larger than that of the hydrogel without biochar. To further understand its swelling behavior, the saturated water content of these hydrogels in pure water and saline solution was recorded (Fig. 2I). The saturated water content of the hydrogel can be calculated using Formula (1):

$$Q = \frac{m_s - m_d}{m_d} \times 100\% \quad (1)$$

where m_s is the mass of hydrogels when swollen to saturation, and m_d is the mass in the dry state. In pure water, the saturated water content of the hybrid hydrogel increased from 217% to 226% compared to the hydrogel. In saline water, the hybrid hydrogel achieved a saturated water content as high as 520% due to its resistance to polyelectrolytes (Peng et al. 2023). The saturated water content of the hybrid hydrogel in saline water was increased by 49% relative to the hydrogel, significantly enhancing its swelling performance.

3.3 The reducted equivalent evaporation enthalpy

The equivalent evaporation enthalpy quantifies the energy required for the evaporation of a unit mass of water and is a crucial parameter for evaluating evaporator performance. As shown in Fig. 3A, compared to direct evaporation of pure water (0.06 kg m^{-2} h^{-1}), the dark evaporation rate of the hydrogel was 0.15 kg m^{-2} h^{-1}, increasing by 1.5 times, illustrating that the hydrogel has a lower evaporation enthalpy due to its unique polymer network structure and ability to activate water molecules (Anukunwithaya et al. 2024). With the incorporation of biochar, the hybrid hydrogel achieved a dark evaporation rate of 0.18 kg m^{-2} h^{-1}, which was 1.2 times that of the hydrogel. It is suggested that biochar promotes the evaporation process of the hydrogel through a non-photothermal mechanism. During the dark evaporation process, both pure water and hydrogels relied on heat from the environment for water evaporation. Therefore, the equivalent evaporation enthalpy of the hydrogel could be obtained by comparing the difference in mass change between the two over the same duration (see Section SI-1 in the Supporting Information for details). Compared to the hydrogel (1052.09 J g^{-1}), the evaporation enthalpy of the hybrid hydrogel was only 877.79 J g^{-1}(Fig. 3B), which is lower than the evaporation enthalpy of most reported hydrogels (Xu et al. 2023; Shu et al. 2024; Chen et al. 2025; Jiang et al. 2025). This indicates that the addition of biochar reduces the equivalent evaporation enthalpy of the hydrogel, making water molecules easier to evaporate under the same energy input, thereby significantly improving dark evaporation efficiency. Differential scanning calorimetry (DSC) can be used to observe the thermal stability of materials. Integrating the DSC curve yields the corresponding evaporation enthalpy. Pure water exhibits a high and sharp endothermic peak near 100 °C (Fig. 3C). In contrast, the DSC curves of the hydrogels present a gradually decaying broad peak with reduced peak height, indicating the weakening of the hydrogen bond network of water molecules (Li et al. 2021b). Figure 3D shows the enthalpy of evaporation calculated from DSC, which displays the same trend as the equivalent enthalpy of evaporation obtained from the latent heat experiment.

Raman spectroscopy was used to evaluate the O–H stretching condition, demonstrating the different states of water molecules in the hydrogels. Water molecules in hydrogels exist in three states: Bound water(BW), Intermediate water (IW), and Free water (FW). IW has weaker interactions with neighbouring water molecules and polymer chains compared to FW and BW,

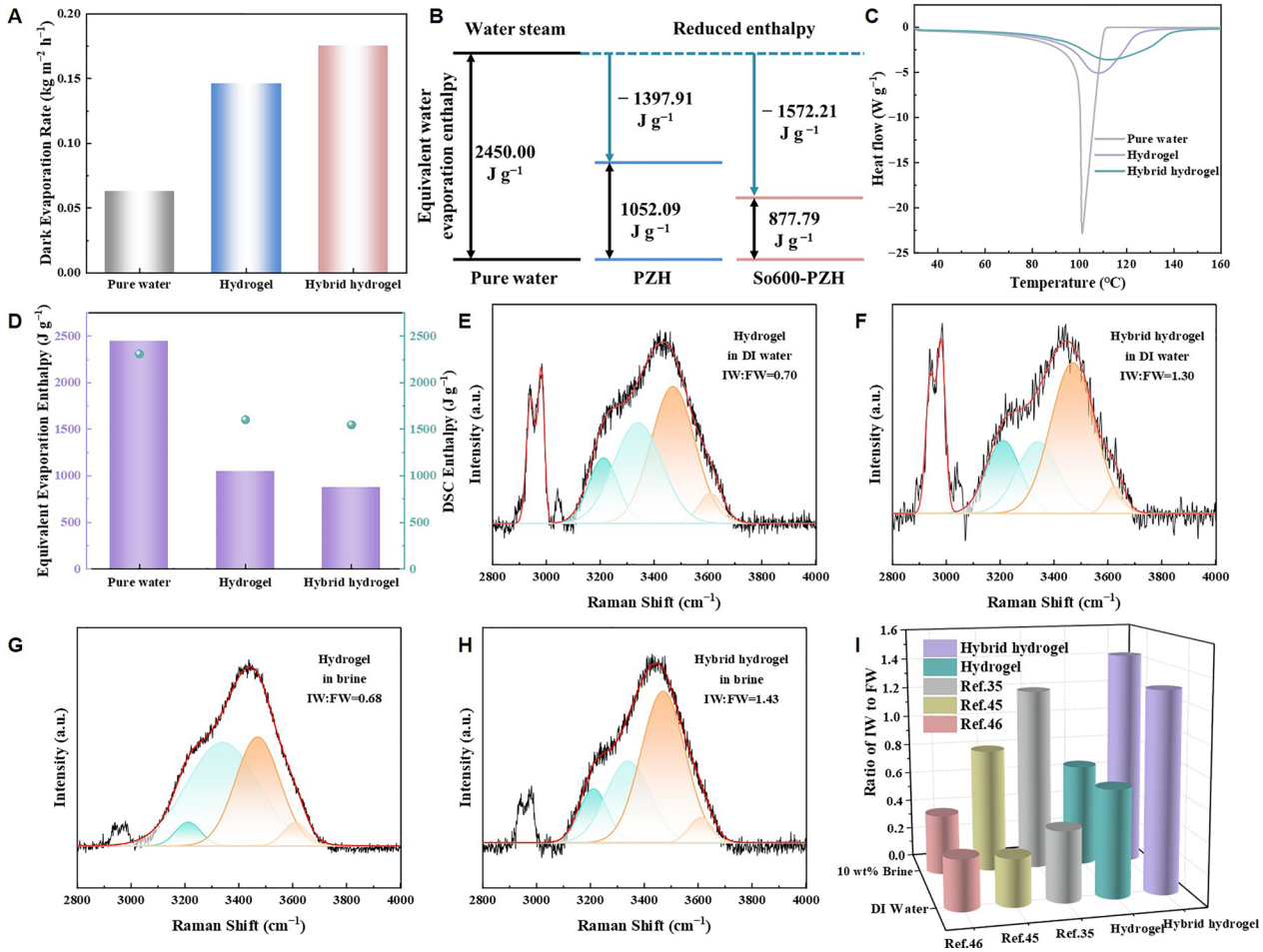

Fig. 3 Activation of water molecules and reduction of enthalpy of hybrid hydrogel. **A** Dark evaporation rate of hydrogel/hybrid hydrogel. **B** Equivalent evaporation enthalpy of hydrogel/hybrid hydrogel. **C** DSC curves of pure water and hydrogels. **D** The enthalpy of evaporation calculated based on the dark experiments and DSC measurements. **E**, **F** Raman spectrum of the hydrogel/hybrid hydrogel in DI water. **G**, **H** Raman spectrum of the hydrogel/hybrid hydrogel in saline water. **I** Comparison of the IW/FW values of hybrid hydrogel in this work with those of some recent hydrogels

and thus requires less energy for evaporation, hence it is also referred to as activated water (Guo et al. 2020). Figure 3E and F show the Raman spectra of the hydrogel and hybrid hydrogel in pure water, respectively. The two peaks at 3212 cm^{-1} and 3340 cm^{-1} correspond to the O–H stretching in FW, which refers to water molecules connected by four hydrogen bonds, with two protons and two lone pair electrons participating in hydrogen bonding. The O–H stretching peaks at 3470 cm^{-1} and 3609 cm^{-1} correspond to IW with weak hydrogen bonding with surrounding water molecules. Through peak fitting and integral calculations, it was found that the IW/FW value of the hydrogel increased from 0.70 to 1.30 due to the incorporation of biochar. The results indicated that biochar significantly affected the hydrogen bond network of water molecules, forming more IW and thereby reducing the equivalent evaporation enthalpy. It could be due to the interaction between the surface functional groups of biochar and the hydrogen bond network, which altered the hydrogen bonding network of water molecules in the hydrogel, promoting the conversion of water molecules from strong hydrogen bonds (FW) to weak hydrogen bonds (IW), thereby further reducing the evaporation enthalpy. Furthermore, Raman testing was conducted on the hydrogel and hybrid hydrogel in saline water, with the results shown in Fig. 3G and H. The IW/FW ratio of the hybrid hydrogel reached as high as 1.43. The C–H bond stretching signal of the hydrogel in the range of 2800–3000 cm^{-1} is greatly weakened, indicating that the polymer chains of the hydrogel became more flexible in saline water, which proves that the salt ions have a shielding effect on the electrostatic interaction in the polyzwitterionic hydrogel (Peng et al. 2023). Compared with those reported in previous studies, as shown in Fig. 3I, the IW/

FW values of the hybrid hydrogel in this study outperform most reported hydrogels in both pure water and saline solutions(Zhu et al. 2020; Lei et al. 2022; Yang et al. 2024)。

4 Conclusions

In this contribution, we revealed the dual-pathway enhancement mechanism of photothermal and non-photothermal performance in hydrogel evaporators through biochar incorporation. Biochar enhanced the hybrid hydrogel's ability to absorb sunlight as a sunlight absorber, concentrating heat within the hydrogel and reducing heat loss to the bulk water, thereby improving the hydrogel's photothermal performance. Additionally, due to the interaction between the surface functional groups of biochar and the groups on the polymer chains of the hydrogel, the pores of the hydrogel became smaller and more uniformly distributed. This increased the opportunity for light absorption and improved the light absorption rate, while also enhancing the capillary force of the pores on water molecules, ensuring an abundant supply of water at the evaporation interface. More importantly, the presence of carboxyl and hydroxyl groups on the biochar surface not only enhanced the hydrogel's hydrophilicity and swelling properties, but also regulated the hydrogen bond network of water molecules within the hybrid hydrogel. It weakened hydrogen bonds, forming more IW, and lowed the evaporation enthalpy of the hydrogel to 877.79 J g^{-1}. Through multi-scale synergy, it boosted the evaporation rate of the hybrid hydrogel to 3.57 kg m^{-2} h^{-1}. Our work provided theoretical guidance and reference for future evaporation applications and further research on hybrid hydrogels.

Supplementary Information

The online version contains supplementary material available at https://doi.org/10.1007/s42773-026-00604-0.

Additional file1 (DOCX 3878 KB)

Author contributions

Sihui Wang: Investigation, Methodology, Writing—Original Draft. Jiaqi Yang: Investigation, Methodology. Aijie Wang: Funding acquisition. Wenzong Liu: Conceptualization, Writing—Review & Editing, Supervision, Funding acquisition. All authors read and approved the final manuscript.

Funding

This research was supported by the National Science Foundation of China (No. 52321005), Shenzhen Science and Technology Program, China (SYSPG20241211173609007), and by the State Key Laboratory of Urban-rural Water Resources and Environment (Harbin Institute of Technology), China (2025DX11).

Data availability

The authors declare that the data supporting the findings of this study are available within the paper and its Supplementary Information files.

Declarations

Competing of interests

The authors declare no competing interests.

Received: 10 November 2025 Revised: 7 January 2026 Accepted: 25 February 2026
Published online: 27 April 2026

References

Aleid S, Wu M, Li R et al (2022) Salting-in effect of zwitterionic polymer hydrogel facilitates atmospheric water harvesting. ACS Mater Lett 4:511–520. https://doi.org/10.1021/acsmaterialslett.1c00723

Alex S, Kumar PR, Chattopadhyay K et al (2019) Thermally evaporated Cu–Al thin film coated flexible glass mirror for concentrated solar power applications. Mater Chem Phys 232:221–228. https://doi.org/10.1016/j.matchemphys.2019.04.078

Anukunwithaya P, Liu N, Liu S et al (2024) Low vaporization enthalpy of modified chitosan hydrogel for high performance solar evaporator. Carbohydr Polym 340:122304. https://doi.org/10.1016/j.carbpol.2024.122304

Bian Y, Shen Y, Tang K et al (2019) Carbonized tree-like furry magnolia fruit-based evaporator replicating the feat of plant transpiration (global challenges 10/2019). Glob Chall 3(10):1970101. https://doi.org/10.1002/gch2.201970101

Chen J, Li H, Chen B et al (2025) Carbon nanotube-wrapped particles in sodium alginate hydrogels for enhanced solar evaporation and EMI shielding through tortuous channel. Int J Biol Macromol 315:144501. https://doi.org/10.1016/j.ijbiomac.2025.144501

Ebrahimi M, Naghali B, Aryanfar M (2022) Thermoeconomic and environmental evaluation of a combined heat, power, and distilled water system of a small residential building with water demand strategy. Energy Convers Manage 258:115498. https://doi.org/10.1016/j.enconman.2022.115498

Fan X, Yang Y, Shi X et al (2020) A MXene-based hierarchical design enabling highly efficient and stable solar-water desalination with good salt resistance. Adv Funct Mater 30:2007110. https://doi.org/10.1002/adfm.202007110

Fan Z, He P, Bai H et al (2024) Green recycling of waste poly(ethylene terephthalate) into Ni-MOF nanorod for simultaneous interfacial solar evaporation and photocatalytic degradation of organic pollutants. Ecomat 6:e12422. https://doi.org/10.1002/eom2.12422

Feng K, Gao N, Zhang W et al (2020) Creation of nonspherical microparticles through osmosis-driven arrested coalescence of microfluidic emulsions. Small 16:1903884. https://doi.org/10.1002/smll.201903884

Ge Y, Wang L, Su Z et al (2024) Efficient solar-driven interfacial water evaporator using hydrogel modified carbon-based biomass with abundant microchannels. Small 20:2309780. https://doi.org/10.1002/smll.202309780

Ghaffar A, Usman M, Khan MU, Hassan M (2024) Simultaneous solar steam and electricity generation from biochar based photothermal membranes. J Cleaner Prod 446:141374. https://doi.org/10.1016/j.jclepro.2024.141374

Gu J, Zhang Y, Xiao P et al (2024) Sunflower-inspired hydrogel evaporator with mutual reinforcement of evaporation and photodegradation for integrated water management. Chem Eng J 490:151550. https://doi.org/10.1016/j.cej.2024.151550

Guo Y, Yu G (2021) Engineering hydrogels for efficient solar desalination and water purification. Acc Mater Res 2:374–384. https://doi.org/10.1021/accountsmr.1c00057

Guo Y, Bae J, Fang Z et al (2020) Hydrogels and hydrogel-derived materials for energy and water sustainability. Chem Rev 120:7642–7707. https://doi.org/10.1021/acs.chemrev.0c00345

Guo Y, Fang Z, Yu G (2021) Multifunctional hydrogels for sustainable energy and environment. Polym Int 70:1425–1432. https://doi.org/10.1002/pi.6271

Guo Y, De Vasconcelos LS, Manohar N et al (2022) Highly elastic interconnected porous hydrogels through self-assembled templating for solar water purification. Angew Chem Int Ed 61:e202114074. https://doi.org/10.1002/anie.202114074

He R, Yuan X, Huang Z et al (2019) Activated biochar with iron-loading and its application in removing Cr (VI) from aqueous solution. Colloids Surf A Physicochem Eng Asp 579:123642. https://doi.org/10.1016/j.colsurfa.2019.123642

Jiang Y, Gong Y, Guo C, Xiang X (2025) Carbon nanotube-nano-Fe3O4 composite graphene hydrogel with optimized 3D structure for high-performance solar evaporation. Desalination 608:118840. https://doi.org/10.1016/j.desal.2025.118840

Lei W, Khan S, Chen L et al (2021) Hierarchical structures hydrogel evaporator and superhydrophilic water collect device for efficient solar steam evaporation. Nano Res 14:1135–1140. https://doi.org/10.1007/s12274-020-3162-5

Lei C, Guan W, Guo Y et al (2022) Polyzwitterionic hydrogels for highly efficient high salinity solar desalination. Angew Chem Int Ed Engl 61:e202208487. https://doi.org/10.1002/anie.202208487

Lei C, Park J, Guan W et al (2023) Biomimetically assembled sponge-like hydrogels for efficient solar water purification. Adv Funct Mater 33:2303883. https://doi.org/10.1002/adfm.202303883

Li J, Zhou X, Chen G et al (2021a) Evaporation efficiency monitoring device based on biomass photothermal material for salt-resistant solar-driven interfacial evaporation. Sol Energy Mater Sol Cells 222:110941. https://doi.org/10.1016/j.solmat.2020.110941

Li W, Tian X, Li X et al (2021b) Ultrahigh solar steam generation rate of a vertically aligned reduced graphene oxide foam realized by dynamic compression. J Mater Chem A 9:14859–14867. https://doi.org/10.1039/D1TA03014K

Li J, Yan L, Li X et al (2022) Porous polyvinyl alcohol/biochar hydrogel induced high yield solar steam generation and sustainable desalination. J Environ Chem Eng 10:107690. https://doi.org/10.1016/j.jece.2022.107690

Li Y-B, Xu L, Han S-J et al (2025) Tea waste biochar hydrogel evaporator with high salt − resistance for highly efficient solar interfacial evaporation. Sep Purif Technol 361:131276. https://doi.org/10.1016/j.seppur.2024.131276

Liu P, Hu Y, Li X-Y et al (2022) Enhanced solar evaporation using a scalable MoS_2-based hydrogel for highly efficient solar desalination. Angew Chem Int Ed 61:e202208587. https://doi.org/10.1002/anie.202208587

Liu G, Zhang B, Zhang X (2025) Fe_3O_4 nanoparticles based dual network microporous hydrogel evaporator for efficient solar water purification. Surf Interfaces 56:105659. https://doi.org/10.1016/j.surfin.2024.105659

Long Y, Huang S, Yi H et al (2019) Carrot-inspired solar thermal evaporator. J Mater Chem A 7:26911–26916. https://doi.org/10.1039/C9TA08754K

Peng B, Lyu Q, Li M et al (2023) Phase-separated polyzwitterionic hydrogels with tunable sponge-like structures for stable solar steam generation. Adv Funct Mater 33:2214045. https://doi.org/10.1002/adfm.202214045

Shu L, Zhang X-F, Wang Z et al (2024) Cellulose-based bi-layer hydrogel evaporator with a low evaporation enthalpy for efficient solar desalination. Carbohydr Polym 327:121695. https://doi.org/10.1016/j.carbpol.2023.121695

Tarek R, Kospa DA, El-Hakam SA et al (2023) Tailoring surface topography of biochar-based hydrogel for hazardous pollutants removal from contaminated seawater through simultaneous steam-electricity generation. Desalination 566:116935. https://doi.org/10.1016/j.desal.2023.116935

Wan H, Fu X, Chen Y et al (2025) Biochar-based hydrogel evaporator with vertically arranged channels for efficient solar steam generation, desalination and water purification. Sep Purif Technol 359:130795. https://doi.org/10.1016/j.seppur.2024.130795

Wang Z, Wu X, Dong J et al (2022) Porifera-inspired cost-effective and scalable "porous hydrogel sponge" for durable and highly efficient solar-driven desalination. Chem Eng J 427:130905. https://doi.org/10.1016/j.cej.2021.130905

Wang P, Cheng J, Luo X et al (2025) Composite distillation membranes with highly water-permeable and anti-crystallization polyzwitterionic layers for deep concentration of hypersaline brine. J Membr Sci 713:123339. https://doi.org/10.1016/j.memsci.2024.123339

Xu N, Hu X, Xu W et al (2017) Mushrooms as efficient solar steam-generation devices. Adv Mater 29:1606762. https://doi.org/10.1002/adma.201606762

Xu J, Wang G, Zhu L et al (2023) Superwetting reduced graphene oxide/alginate hydrogel sponge with low evaporation enthalpy for highly efficient solar-driven water purification. Chem Eng J 455:140704. https://doi.org/10.1016/j.cej.2022.140704

Yang Q, Ma X, Li Y et al (2023) One-pot pyrolysis and enhanced efficient solar evaporation of Cu/Cu2O/biochar. Mater Today Sustain 22:100363. https://doi.org/10.1016/j.mtsust.2023.100363

Yang H, Hu Z, Huang Z et al (2024) Three-dimensional zwitterionic hydrogel-based evaporators with simultaneous ultrahigh evaporation rates and anti-fouling performance. Nano Energy 127:109784. https://doi.org/10.1016/j.nanoen.2024.109784

Yu X, Fang J, Kong X et al (2025) Superabsorbent hydrogel evaporator with sandwich SA/CNTs/SA cellular wall for solar-driven water purification. Chem Eng J 505:159893. https://doi.org/10.1016/j.cej.2025.159893

Zhang YS, Khademhosseini A (2017) Advances in engineering hydrogels. Science 356:eaaf3627. https://doi.org/10.1126/science.aaf3627

Zhang Q, Zhang Y, Shen Y et al (2021) Improving seawater desalination efficiency by solar driven interfacial evaporation based on biochar evaporator of *Nannochloropsis oculata* residue. J Environ Chem Eng 9:105787. https://doi.org/10.1016/j.jece.2021.105787

Zhang Q, Yang X, Deng H et al (2022a) Carbonized sugarcane as interfacial photothermal evaporator for vapor generation. Desalination 526:115544. https://doi.org/10.1016/j.desal.2021.115544

Zhang Q, Ye Q, Zhang Y et al (2022b) High efficiency solar interfacial evaporator for seawater desalination based on high porosity loofah sponge biochar. Sol Energy 238:305–314. https://doi.org/10.1016/j.solener.2022.04.044

Zheng SY, Zhou J, Si M et al (2023) A molecularly engineered zwitterionic hydrogel with strengthened anti-polyelectrolyte effect: from high-rate solar desalination to efficient electricity generation. Adv Funct Mater. https://doi.org/10.1002/adfm.202303272

Zhu F, Wang L, Demir B et al (2020) Accelerating solar desalination in brine through ion activated hierarchically porous polyion complex hydrogels. Mater Horiz 7:3187–3195. https://doi.org/10.1039/D0MH01259A